Structural Studies of Aqueous Solutions by the Anomalous X-ray Scattering Method

Eiichiro Matsubara[1] and Kozo Shinoda[2]

[1]*Department of Materials Science and Engineering, Graduate School, Kyoto University, Kyoto 606-8501, Japan*
[2]*Institute for Advanced Materials Processing, Tohoku University, Sendai 980-8577, Japan*

ABSTRACT

The atomic scale structure of solutions has been recognized as one of the most important research subjects in both aqueous solution chemistry and hydrometallurgy. For this purpose, knowledge of the environmental structure around a certain metallic cation in solution is strongly required. The anomalous x-ray scattering (AXS) method, particularly, the energy derivative AXS method, enables us to reduce difficulties due to corrections for scattering from a solution cell as well as for large contribution from water molecules. An attempt is made in this paper to review current studies of hydration structures in concentrated chloride solutions, local structures of ferric hydroxide gel, and atomic structures of poly-molybdate ions in acid Mo-Ni aqueous solutions.

1. INTRODUCTION

The energy derivative anomalous x-ray scattering method (hereafter referred to as "the AXS method") is based on the idea proposed by Hosoya /1/ and Shevchik /2/, which was first used by Fuoss *et al* /3/ with synchrotron radiation at Stanford University under the name of differential anomalous scattering (DAS). On the other hand, a goniometer system for the AXS measurements have exclusively built in the Photon Factory (PF) of High Energy Accelerator Research Organization (KEK), Tsukuba, Japan /4/. The advantage of the AXS method is that we can obtain a chemical environment around a specific element /5/. For lack of chemical selectivity, a structure around a metallic cation in aqueous solution is hardly determined by both conventional x-ray and neutron diffraction. For example, in a metal-halide solution, such as $ZnCl_2$-H_2O system, the total structure factor by the conventional method is a sum of ten partial structure factors, which contains a large contribution of the partial structure factor of O-O pairs. In this regard, the environmental structure factor by the AXS method consists of only four partial structure factors without a large contribution from water molecules /6,7/. This enables us to evaluate a precise atomic structure around a metallic cation in a solution.

As synchrotron radiation source of x-rays has become more accessible, the AXS method has been receiving much attention, although its application to aqueous solutions is still very limited.

In this paper, we will present some selected experimental results for three different types of aqueous solutions by the AXS method. This includes a simple example of the hydration structure in concentrated $ZnCl_2$ solutions /6/, and more complicate systems of the ferric hydroxide gel in solution /8/ and poly-molybdate ions in acid Mo-Ni solutions /9/, in order to demonstrate a potential of the AXS method.

2. FUNDAMENTALS OF THE AXS ANALYSIS

The total x-ray atomic scattering factor f is expressed by $f = f_0 + f' + i f''$, using the usual atomic scattering factor f_0 at an energy sufficiently away from the absorption edge, and the real and imaginary parts of the anomalous dispersion terms (ADTs) f' and f''. The ADTs show a drastic change only near the absorption edge. Fig.1 shows the ADTs of Zn /5/ theoretically calculated by Cromer and Liberman's method /10/ together with the values experimentally determined

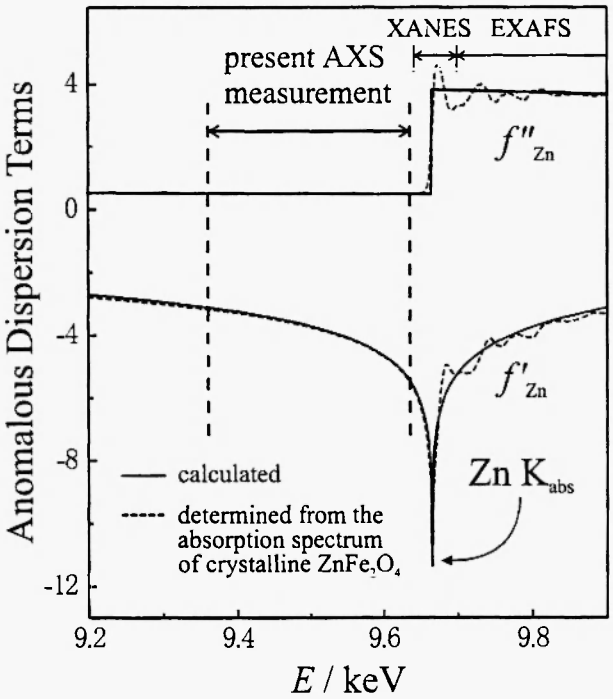

Fig. 1: Energy dependence of the real and imaginary parts of anomalous dispersion terms of Zn.

from the absorption coefficient measurement for crystalline $ZnFe_2O_4$ /11/, as a function of energy. The theoretical values do not coincide with the experimental ones at the higher energy side because of the presence of the x-ray absorption fine structure and the x-ray absorption near edge structure. Furthermore, at the higher energy side, a small intensity difference due to the ADT is hardly detected because of large background by the fluorescent radiation. Thus, a large change of f' at the lower energy side of the absorption edge is used in the present AXS method. Further details of the experimental setting and analysis in the present AXS method with the synchrotron radiation in the PF have been given in /4/. Only some essential points are given below.

When the incident energy is selected in the close vicinity of the absorption edge of a certain element, for example the A-component, the detected variation in intensity $\Delta i_A(Q)$ can be attributed only to the change of the anomalous dispersion terms of the A-component, f'_A and f''_A. Furthermore, in the lower energy side of the absorption edge, we have only to consider the energy dependence in intensity due to the real part f'_A. Therefore, the following relation is readily obtained/12/:

$$\Delta i_A(Q) = \frac{\{I(Q,E_1) - \langle f^2(Q,E_1)\rangle\} - \{I(Q,E_2) - \langle f^2(Q,E_2)\rangle\}}{c_A\{f_A(E_1) - f_A(E_2)\}W(Q)}$$

$$= \int_0^\infty 4\pi r^2 \sum_k^{elements} \frac{\Re\{f_k(Q,E_1) + f_k(Q,E_2)\}}{W(Q)}(\rho_{Ak}(r) - \rho_{0k})\frac{\sin(Qr)}{Qr}dr, \quad (1)$$

$$W(Q) = \sum_k^{elements} c_k \Re\{f_k(Q,E_1) + f_k(Q,E_2)\},$$

where $E_{abs}>E_2>E_1$, $I(Q,E)$ is the coherent X-ray scattering intensity in electron units per atom, c_k the atomic fraction of the k-element, $\rho_{Ak}(r)$ the radial density function of the k-element around the A element at a radial distance of r, and ρ_{0k} is the average number density of the k-element in the system. $\Re$ denotes the real part of the values in the brackets. The environmental radial distribution function (RDF) for A is estimated by Fourier transformation of the differential quantity of $\Delta i_A(Q)$ in eq.(1).

$$4\pi r^2 \rho_A(r) = 4\pi r^2 \rho_0 + \frac{2r}{\pi}\int_0^\infty Q\Delta i_A(Q)\sin(Qr)dQ, \quad (2)$$

where ρ_0 is the average number density in the system. Consequently, the environmental structure around a specific element can be obtained by measuring the energy dependence of the X-ray scattering intensity with more than two energies in the close vicinity of the absorption edge of a desired element.

The use of the AXS method also has another merit, especially in the experiments for solutions. For diffraction experiments, a solution is usually contained in a cell with windows transparent for x-rays. For quantitative structural analyses, intensity from a solution should be accurately corrected for scattering intensity from the window materials. This is usually carried out using the intensity only from the window materials corrected for absorption by solution. Each scattering intensity profile contains the contribution from the window materials as well as from the solution. By taking a difference between the two profiles, however, the contribution from the window materials as well as that from the none zinc pairs is automatically eliminated, as given in the schematic diagram of Fig.2.

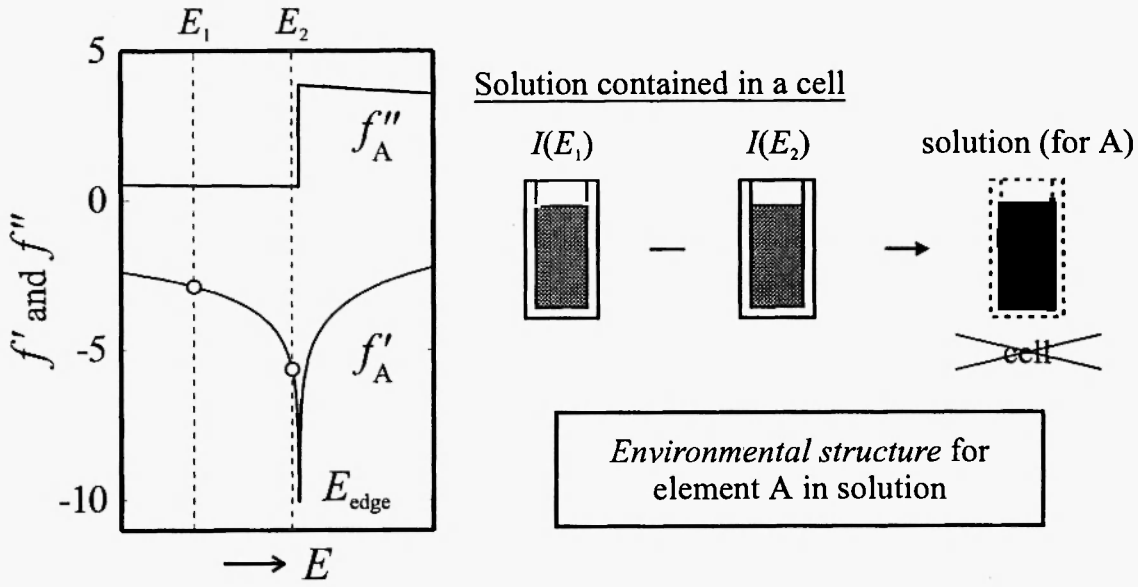

Fig. 2: Schematic diagram for the application of AXS to the measurement for solution contained in a cell.

In this way, we can release from the tedious correction procedure for the window materials. This process was developed by analogy of the AXS measurement in an amorphous thin film grown on a substrate /12,13/.

3. HYDRATION STRUCTURE OF ZNCL$_2$ AQUEOUS SOLUTION

The intensity profiles of 0.98 and 2.85mol/l $ZnCl_2$ aqueous solutions measured at energies of 9.361 and 9.636keV just below the Zn K absorption edge (9.660keV) are shown in Fig.3 (a) and (c), respectively. The energy differential profile between the two intensities ΔI_{Zn} in each solution is also shown in Fig.3 (b) and (d). The intensity ΔI_{Zn} is due to the difference of f'_{Zn} at two energies indicated with broken lines in Fig.1. By analyzing ΔI_{Zn}, we can extract the structural information around a Zn ion in these solutions. The differential interference function $Q\Delta i_{Zn}(Q)$ is calculated from ΔI_{Zn} and then the environmental radial distribution function (RDF) around Zn ion can be calculated by using the Fourier transformation of $Q\Delta i_{Zn}(Q)$.

The environmental RDFs for Zn ions in 0.98 and 2.85mol/l $ZnCl_2$ solutions are shown with the total RDFs obtained by the conventional diffraction method in Fig.4. The peak at about 0.3nm in the total RDFs,

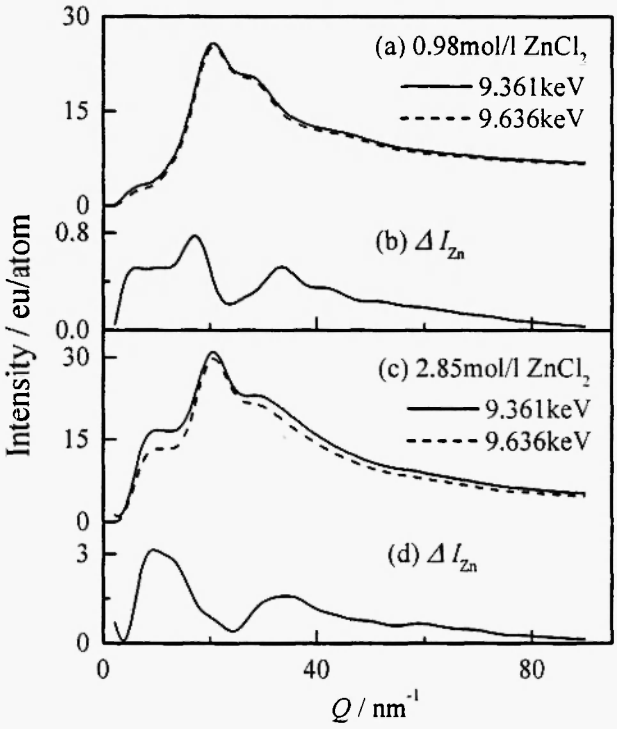

Fig. 3: Intensity profiles measured at 9.361 (solid curve) and 9.636 (broken curve) keV in the (a) 0.98 and (b) 2.85 mol/l $ZnCl_2$ aqueous solutions. The differential profiles in the solutions (a) and (b) are shown in (c) and (d) respectively.

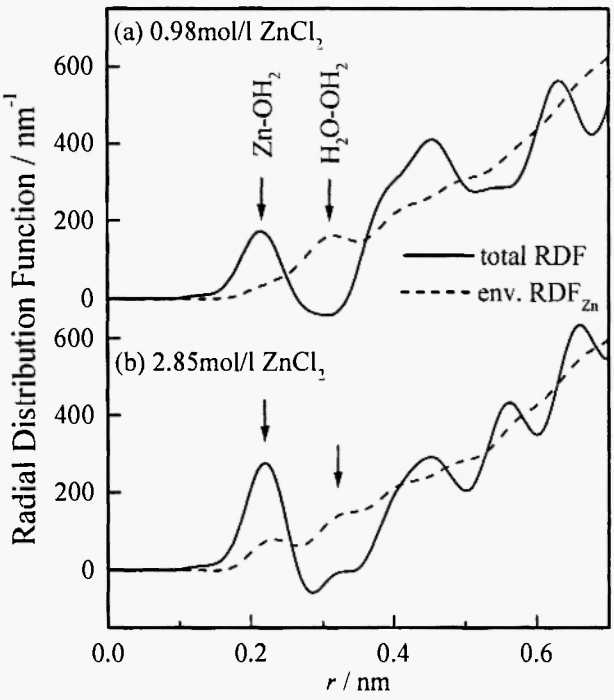

Fig. 4: Environmental RDFs for Zn ions (solid curves) and total RDFs (broken curves) in (a) 0.98 and (b) 2.85 mol/l $ZnCl_2$ aqueous solutions.

which is ascribed to O-O pairs of water molecules /14/ and Cl^--O pairs of a water molecule hydrated around a chrolide ion /15/, disappears in the environmental RDFs. Referring to the reported distance between a zinc ion and oxygen of hydrated water molecules, the hydration number and distance of Zn ions are estimated from the first peak in the environmental RDF. The hydration numbers for a Zn ion are 5.7±0.7 at 0.210±0.002nm in the 0.98mol/l $ZnCl_2$ solution and 6.2±0.2 at 0.215±0.002nm in the 2.85mol/l $ZnCl_2$ solution /6/. According to some EXAFS studies /16,17/, there are some tetrahedral complexes around a zinc ion in concentrated aqueous solutions. The present results, however, rather support the results by the conventional x-ray scattering method than those by the EXAFS. Namely, the hydration number of a Zn ion is about 6 and the hydration distance is about 0.210nm /18-22/. The present results also indicate that the hydration structure around a Zn ion shows any significant change even in the 2.85mol/l $ZnCl_2$ solution.

The hydration structure of a heavier element, such as Er, has also been determined by the AXS method using the L_{III} absorption edge instead of the K absorption edge. Since the magnitude of f' is about three times larger at the L_{III} absorption edge than at the K absorption edge, a larger intensity difference is achieved by using the L_{III} absorption edge instead of the K absorption edge. This sometimes enables us to obtain the AXS data even from an element of less concentration /7/.

4. FERRIC HYDROXIDE GEL

Various iron oxides, oxyhydroxides and hydroxides are widely distributed in soils, minerals, rivers, sea water, etc., and playing an important role in our environment, biological actions and industrial activities. The formation and transformation of iron (hydrous) oxides in aqueous solutions are reviewed /23/. Little is, however, known about the atomic structure of ferric hydroxides in the early stage of the hydrolytic behavior of ferric ions. The atomic scale structure of hydroxides in water is often evaluated from the freeze-dried powder sample on the assumption that their atomic structures are identical. In this example, the structure of the ferric hydroxide gel in aqueous solution was investigated by the AXS method at the Fe K absorption edge.

Intensities of the ferric hydroxide gel observed at 7.086 and 6.811keV below the Fe K absorption edge (7.111keV) are shown in Fig.5 (a). Their intensity difference in (b) is compared with the intensity of the freeze-dried $Fe(OH)_3$ powder in (c). Diffuse peaks of the powder sample indicated with small arrows in (c) are also observed in the differential intensity profile of the gel in (b). This suggests that the fundamental atomic structure in the gel resembles that in the powder.

According to Narten and Levy /24/, the interference functions is given by

$$Qi(Q) = \sum_{j=1}^{n}\sum_{k=1}^{n'} c_j N_{jk} e^{-b_{jk}Q^2} \frac{f_j f_k}{<f>^2} \frac{\sin(Qr_{jk})}{r_{jk}} \quad (3)$$

$$+4\pi\rho_o \times \sum_{j=1}^{n}\sum_{k=1}^{n} e^{-B_{jk}Q^2} \frac{c_j c_k f_j f_k}{<f>^2} \frac{QR_{jk}\cos(QR_{jk}) - \sin(QR_{jk})}{Q^2}$$

where $Q=4\pi\sin\theta/\lambda$. The term n is the number of elements, n' the number of j-k pairs taken into account

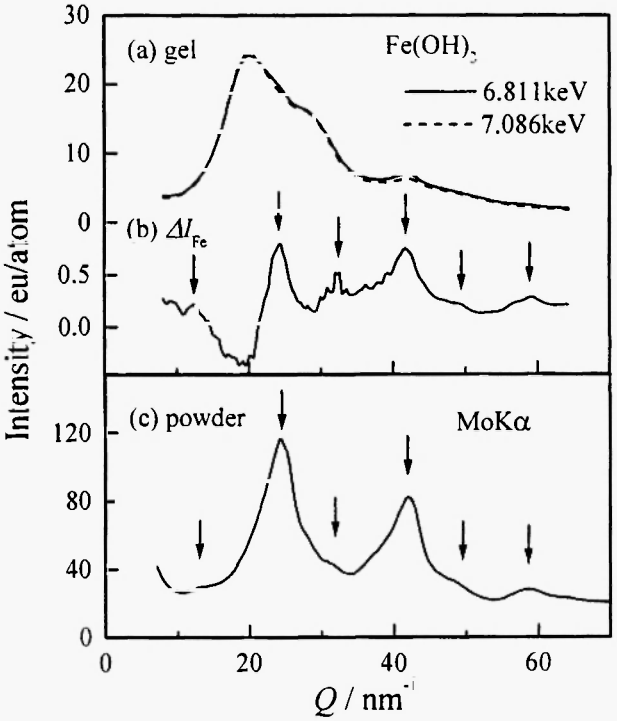

Fig. 5: (a) Scattering intensity profiles observed at 6.811 (solid curve) and 7.086 (broken curve) just below the Fe K absorption edge in the gel, (b) their differential intensity profile, and (c) scattering intensity in the powder by Mo Kα radiation

in the calculation, N_{jk} the coordination number of *j-k* pairs at the distance r_{jk}, and b_{jk} the mean square variation The quantities of R_{jk} and B_{jk} represent the mean and variance of the boundary region, which need not be sharp. In practice, the distance and coordination numbers of near neighbor pairs are obtained by the least-squares calculation of eq.(3) so as to reproduce the experimental interference function /24,25/. The differential interference function obtained by the AXS method is readily calculated by taking the difference between two interference functions in eq.(3) evaluated at two energies below the absorption edge /26/. Using this least-squares variational method, we determined the coordination numbers and atomic distances around a ferric ion in Table 1. The observed and calculated differential interference function of the gel and the total interference function of the powder are shown in Fig.6. In comparison between the gel and the powder, no significant difference except for the coordination number of the second neighbor Fe-Fe pair is observed. This coordination number is about 60% less in gel than in the powder.

The crystalline structures of ferric hydroxides and oxides have common structural features that the fundamental structural unit is FeO_6 octahedra and a linkage between these octahedra is classified into four different types in Fig.7. An average distance between ferric ions is different in every type of linkage, that is, 0.289nm for the face-sharing linkage in (a), 0.297 to 0.308nm for the edge-sharing linkage in (b), 0.337 to 0.370nm for the double-corner sharing linkage in (c), and 0.390nm for the single-corner sharing linkage. The coordination numbers of oxygen around a ferric ion are 5.5±0.5 at 0.209±0.002nm in the gel and 5.5±0.3 at 0.199±0.002nm in the powder. This indicates that the fundamental unit structure is FeO_6 octahedra common to other ferric hydroxides and oxides. Comparing the distances between ferric ions in Table 1 with those of four types in Fig.7, we conclude that the types of linkage between the FeO_6 octahedra are considered the edge-sharing or double-corner sharing linkage and there is neither face- nor single-corner sharing type. The increase in the coordination numbers of ferric ion pairs at the longer distance in the powder manifests the

Table 1

Coordination numbers and atomic distances determined in the ferric hydroxide gel by the AXS method at the Fe K absorption edge and in the freeze-dried powder by the conventional x-ray diffraction method /8/

Pair	gel		powder	
	r / nm	*N*	*r* / nm	*N*
Fe-O(1)	0.209	5.5	0.199	5.5
Fe-O(2)	0.367	7.0	0.365	8.5
Fe-Fe(1)	0.316	3.6	0.308	3.9
Fe-Fe(2)	0.341	2.2	0.344	3.6

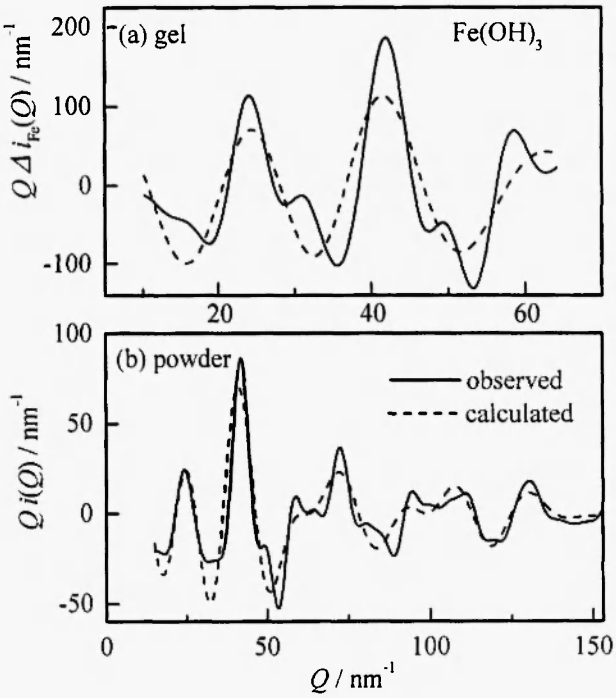

Fig. 6: The differential interference function for ferric ions in the gel and the interference function in the powder. Dashed curves represent the calculated inteference functions by the least-squares variational method.

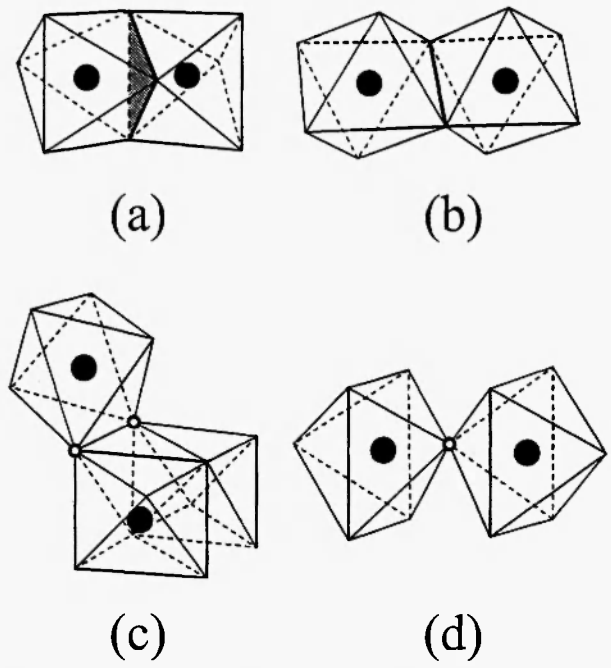

Fig. 7: Schematic drawings of the four types of linkage between FeO_6 octahedra in ferric hydroxides and oxides; (a) face-, (b) edge-, (c) double-corner, and (d) single-corner sharing linkages.

increase in the number of the double-corner sharing linkage. Therefore, in gel, the double-corner sharing linkage is partially broken due to the presence of water molecules. In freeze-drying process, these water molecules are removed from the structure, which completes the double-corner sharing linkage and forms the network structure consisting of the edge- and double-corner sharing FeO_6 octahedra in the powder form.

5. POLY-MOLYBDATE COMPLEXES IN ACID MO-NI SOLUTION

Electrodeposited Mo-Ni alloys /27/ show the superior corrosion and wear resistance. Their catalytic activity in the industrial production of hydrogen from alkaline-water electrolytic cells is also notable /28/. In addition to this practical relevance, the electrodeposition of molybdenum alloy is of considerable interest from a scientific point of view. Pure molybdenum is not electrodeposited from an aqueous solution. It is electrically codeposited only from an aqueous solution containing an iron-group metal. Brenner /29/ described the electrodeposition of these alloys as induced codeposition. In spite of several theoretical hypotheses /30-34/, the mechanism of induced codeposition has not been well understood yet. With this subject, the atomic scale structures of molybdenum and nickel ions in the Mo-Ni aqueous solutions have recently been obtained by applying the AXS and EXAFS methods. This is a new fundamental approach for understanding the mechanism of the induced codeposition.

Similar structural information around a particular element is known to be obtained from the AXS and EXAFS methods. The EXAFS method is especially sensitive in the first nearest neighbor pairs. On the other hand, the AXS method gives structural information for atomic pairs even at a longer distance. For this reason, the structural parameters for adjacent Mo-O and Ni-O pairs at the first nearest neighbor distance are

determined by the EXAFS method. Using such EXAFS data for Mo-O and Ni-O pairs, the structural parameters for neighboring Mo-Mo and Mo-Ni pairs at a longer distance are then determined by the least squares variational method in eq.(3) coupled with the differential interference functions by the AXS method /26/.

Fig.8 gives the Fourier transforms of weighted EXAFS spectra for Mo ions in 1.0mol/l Na_2MoO_4, 0.5mol/l Na_2MoO_4 + 0.5mol/l $NiSO_4$, and 0.5mol/l Na_2MoO_4 + 0.5mol/l $NiSO_4$+1.0mol/l Na_3 cit. aqueous solutions. No significant difference is detected in the peaks at about 0.12 and 0.18nm in Fig.8(a) to (c) in all solutions. Thus, these Mo radial structure functions (RSFs) indicate that the first shells around Mo ions are not influenced by other ionic species. Coordination numbers and atomic distances for the first shell around Mo ions were determined by the Fourier-filtering method of EXAFS. The region denoted by the dotted lines in Fig.8 corresponds to the width of a window function used for filtering the first neighboring shell.

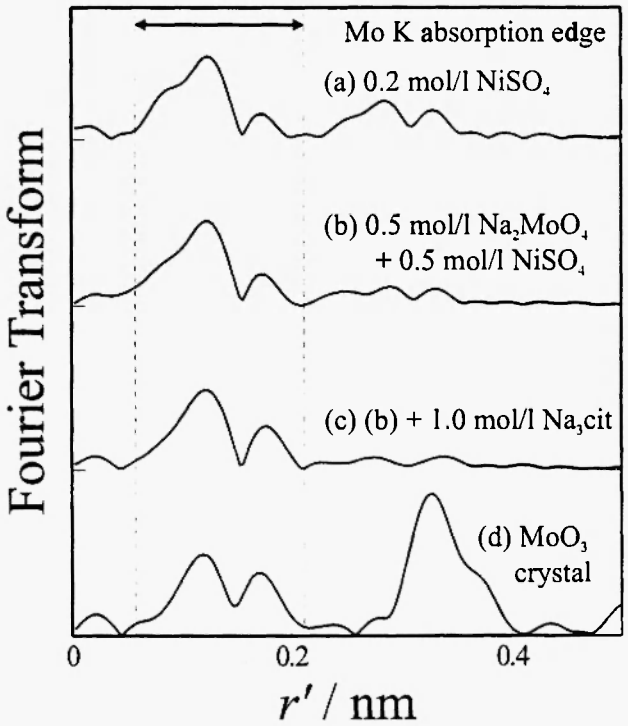

Fig. 8: Fourier transforms of weighted EXAFS spectra in (a) 1.0 mol/l Na_2MoO_4, (b) 0.5 mol/l Na_2MoO_4 + 0.5 mol/l $NiSO_4$, and (c) 0.5 mol/l Na_2MoO_4 + 0.5 mol/l $NiSO_4$ + 1.0 mol/l Na_3 cit. aqueous solutions, and (d) MoO_3 crystal.

The Fourier-filtered Mo EXAFS spectra $k^3\chi$(k) are given by the solid curves in Fig.9. On the other hand, the dashed curves in Fig.9 are the values estimated from the structural parameters in Table 2. It is worth noting that a model with three Mo-O pairs with different distances is required to fully fit the Mo EXAFS spectra in Fig.9. This is verified by the EXAFS spectrum of crystalline MoO_3 in Fig.9 (d). According to the crystalline molybdenum trioxide MoO_3 data /35/, the

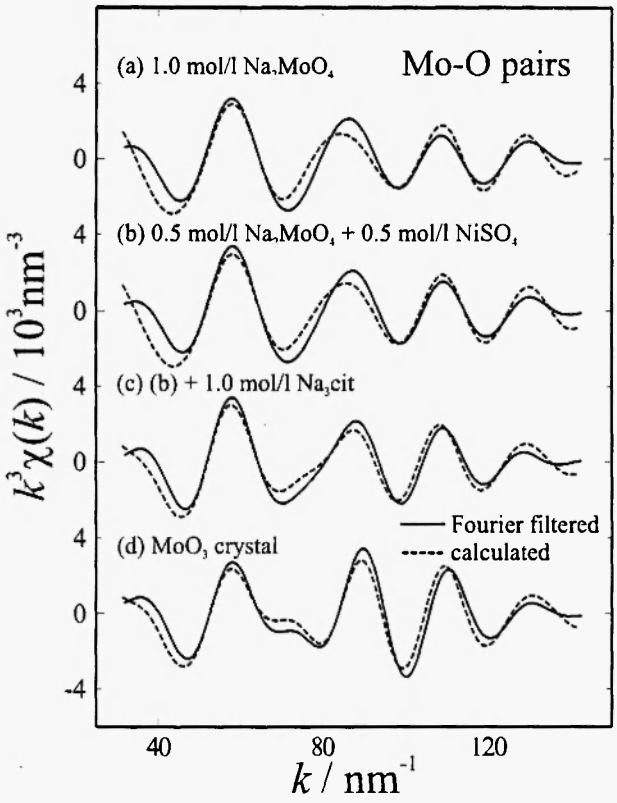

Fig. 9: Fourier-filtered Mo EXAFS spectra in (a) 1.0 mol/l Na_2MoO_4, (b) 0.5 mol/l Na_2MoO_4 + 0.5 mol/l $NiSO_4$, and (c) 0.5 mol/l Na_2MoO_4 + 0.5 mol/l $NiSO_4$ + 1.0 mol/l Na_3 cit. aqueous solutions, and (d) MoO_3 crystal. The dashed lines denote the values calculated from the data of Table 2.

structural unit is a distorted octahedron consisting of a molybdenum atom surrounded by 6 oxygen atoms. These 6 oxygen atoms are grouped by 2's with 3 different Mo-O distances of 0.167-0.173, 0.195 and 0.225-0.233nm. These values are consistent with the present EXAFS results in crystalline MoO_3 in Table 2.

Table 2

Coordination numbers and atomic distances in the first shell determined from the Mo EXAFS spectra in 1.0mol/l Na_2MoO_4, 0.5mol/l Na_2MoO_4 + 0.5mol/l $NiSO_4$, and 0.5mol/l Na_2MoO_4 + 0.5mol/l $NiSO_4$ + 1.0mol/l Na_3 cit. aqueous solutions, and MoO_3 crystal /9/. Their experimental errors are ±0.2 and ±0.002nm, respectively.

Aqueous solution	Mo-O(1)		Mo-O(2)		Mo-O(3)	
	r / nm	*N*	*r* / nm	*N*	*r* / nm	*N*
1.0mol/l Na_2MoO_4	0.173	2.1	0.193	2.0	0.224	2.0
0.5mol/l Na_2MoO_4+0.5mol/l $NiSO_4$	0.172	2.1	0.192	2.2	0.223	1.9
0.5mol/l Na_2MoO_4+0.5mol/l $NiSO_4$ + 1.0mol/l Na_3 cit.	0.172	2.0	0.194	2.1	0.228	2.0
MoO_3 crystal	0.170	2.0	0.194	2.0	0.229	2.0

Consequently, the Mo EXAFS spectra in these solutions in Fig.9 were also analyzed with the model of three Mo-O distances as it is seen in Table 2. This clearly supports that the Mo ions form the distorted MoO_6 octahedra even in the solutions.

Environmental RDFs for Mo ions were determined by the AXS method in 1.0mol/l Na_2MoO_4, 0.5mol/l Na_2MoO_4 + 0.5mol/l $NiSO_4$, and 0.5mol/l Na_2MoO_4 + 0.5mol/l $NiSO_4$+1.0mol/l Na_3 cit. aqueous solutions. The results are shown in Fig.10. From the structural data of Mo-O pairs in the near neighbor region listed in Table 2, we find that the two peaks at about 0.18 and 0.23nm in the RDFs in Fig.10 are attributed to the overlapped Mo-O(1) and Mo-O(2) pairs, and the Mo-O(3) pairs, respectively. As clearly seen in Fig.8, the solutions do not show any distinct peak at about 0.33nm in Fig.8 where an apparent peak of Mo-Mo pairs is observed in the MoO_3 crystal. Quantitative analysis of Mo-Mo(Ni) pairs in the solutions is very difficult from the EXAFS data alone. On the other hand, the distinct peak of Mo-Mo(Ni) pairs is observed at about 0.33nm in the environmental RDFs for Mo in Fig.10. Thus, the structural parameters for Mo-Mo(Ni) pairs in these solutions were accurately determined from the AXS data at Mo K absorption edge. In combination with the structural parameters for the Mo-O pairs in Table 2 and the differential interference function for Mo, $Q\Delta i_{Mo}(Q)$ obtained by the AXS method in Fig.11, the coordination numbers and atomic distances at about

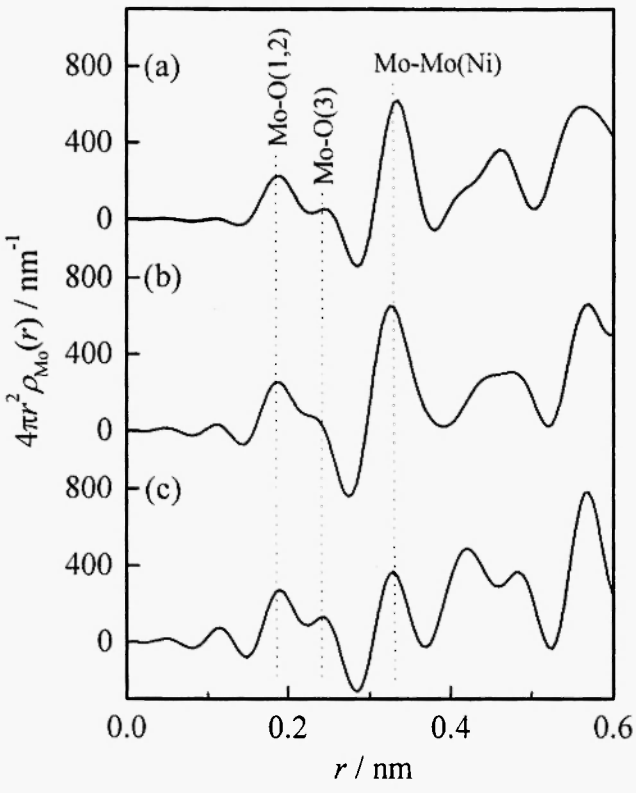

Fig. 10: Environmental radial distribution functions around Mo ions, $4\pi r^2 \rho_{Mo}(r)$ in (a) 1.0 mol/l Na_2MoO_4, (b) 0.5 mol/l Na_2MoO_4 + 0.5 mol/l $NiSO_4$, and (c) 0.5 mol/l Na_2MoO_4 + 0.5 mol/l $NiSO_4$ + 1.0 mol/l Na_3 cit. aqueous solutions.

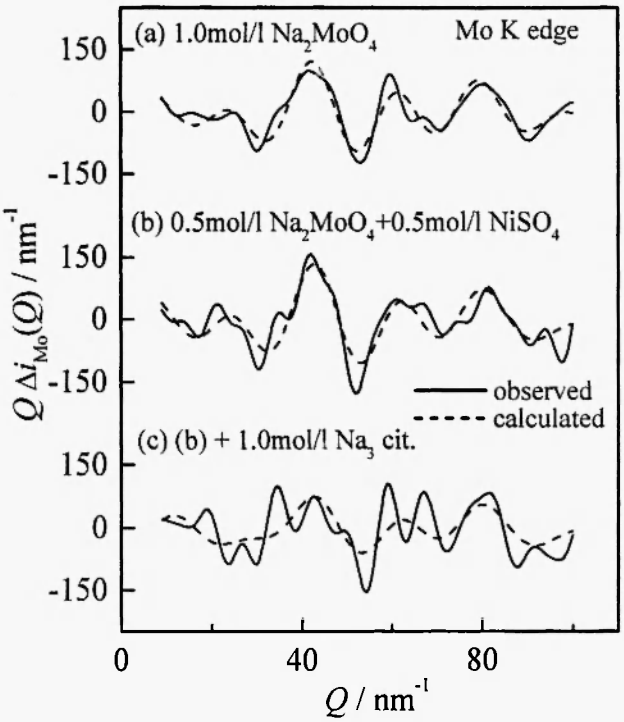

Fig. 11: Differential interference functions $Q\ \Delta I_{Mo}(Q)$ of (a) 1.0 mol/l Na_2MoO_4, (b) 0.5 mol/l Na_2MoO_4 + 0.5 mol/l $NiSO_4$, and (c) 0.5 mol/l Na_2MoO_4 + 0.5 mol/l $NiSO_4$ + 1.0 mol/l Na_3 cit. aqueous solutions determined by the AXS method at Mo K absorption edge. Dashed curves represent the calculated interference functions by the least-square variational method.

0.33nm were determined by the least-squares variational method. The resultant structural parameters for Mo-Mo(Ni) pairs are summarized in Table 3.

The structural unit in the 1.0mol/l Na_2MoO_4 solution is considered to be the distorted MoO_6 octahedron which is similar to the one in the MoO_3 crystal. Since the atomic distance of Mo-Mo pairs in the Na_2MoO_4 solution is 0.335nm in Table 3, the MoO_6 octahedra appear to be connected by sharing their edges. Because of coincidence between the data of Mo-Mo pairs in the Na_2MoO_4 solution and the crystalline $Na_6Mo_7O_{24}14H_2O$ case /36/, it is likely that the local ordering structure consisting of the MoO_6 octahedra is close to the cluster in the crystal. Accordingly, molybdenum ions in the 1.0mol/l Na_2MoO_4 solution form poly-molybdate ions as illustrated in Fig.12(a). Such poly-molybdate ions are composed of 7 MoO_6 octahedra which are connected by sharing their edges. This is consistent with the fact /37,38/ that molybdenum ions are mainly form $Mo_7O_{24}^{6-}$ oxo-complexes consisting of 7 MoO_6 octahedra in an acid molybdate aqueous solution.

The structural unit of MoO_6 octahedron is not changed regardless of the presence of Ni ions as it is clearly seen in Table 2. We can find in Table 3 that the coordination numbers and atomic distances of Mo-Mo and Mo-Ni pairs in the 0.5mol/l Na_2MoO_4 + 0.5mol/l $NiSO_4$ solution agree well with the values of the $Na_3(CrMo_6O_{24}H_6)8H_2O$ crystal /39/. Thus, it is plausible that all Mo ions and a part of Ni ions form a poly-molybdate ion in Fig.12(b) which corresponds to a cluster found in the $Na_3(CrMo_6O_{24}H_6)8H_2O$ crystal in spite of the difference between Ni and Cr. This result is also confirmed that the $Na_3(CrMo_6O_{24}H_6)8H_2O$ single crystal was grown from an aqueous solution containing Na_2MoO_4 and $Cr(NO_3)_3$ at a 6 to 1 ratio with the pH of 4.5 /39/.

We notice in Fig.10 that the peak height due to Mo-Mo(Ni) pairs at about 0.33nm is reduced in the solution containing citric ions. Although the total number of Mo and Ni around Mo at 0.33nm is 3.4 in the 0.5mol/l Na_2MoO_4 + 0.5mol/l $NiSO_4$ solution, it becomes 1.4 by adding the 1.0mol/l Na_3 citrate to the solution. This implies that clusters with the relatively larger size are likely to present in the 0.5mol/l Na_2MoO_4 + 0.5mol/l $NiSO_4$ solution and only small ones are in the 0.5mol/l Na_2MoO_4 + 0.5mol/l $NiSO_4$ + 1.0mol/l Na_3 cit. solution. Taking account of a decrease in the total coordination numbers around Mo in Table3, we readily conclude that the large poly-molybdate ions in Fig.12(b) are decomposed into small molybdate ions consisting of a few MoO_6 octahedra at most by adding citric ions to the 0.5mol/l Na_2MoO_4 + 0.5mol/l $NiSO_4$ solution. The mechanism of this decomposition process is probably explained by the following. Since nickel ions form complexes with citric ions, the large poly-molybdate ions containing nickel ion are decomposed when adding citrates. It is worth mentioning that the small-angle x-ray scattering measurement from these solutions also supports the decomposition of the large poly-molybdate ions under the presence of citric ions /9/.

Molybdenum is electrodeposited only from solutions

Table 3

Coordination numbers and atomic distances of Mo-Mo and/or Mo-Ni pairs in 1.0mol/l Na_2MoO_4, 0.5mol/l Na_2MoO_4 + 0.5mol/l $NiSO_4$, and 0.5 mol/l Na_2MoO_4 + 0.5mol/l $NiSO_4$ + 1.0mol/ Na_3 cit. aqueous solutions /9/. Their experimental errors are ±0.2 and ±0.002nm, respectively. Coordination numbers and atomic distances of Mo-Mo and Mo-Ni pairs in crystalline $Na_6Mo_7O_{24}14H_2O$ /34/ and $Na_3(CrMo_6O_{24}H_6)8H_2O$ /37/ are also included.

Sample	Mo-Mo		Mo-Ni	
	r / nm	*N*	*r* / nm	*N*
1.0mol/l Na_2MoO_4 sol.	0.335	2.9	-	-
0.5mol/l Na_2MoO_4+0.5mol/l $NiSO_4$ sol.	0.329	2.1	0.331	1.3
$Na_6Mo_7O_{24}14H_2O$ crystal	0.333	3.1	-	-
$Na_3(CrMo_6O_{24}H_6)8H_2O$ crystal	0.333	2.0	0.333	1.0

	Mo-Mo(Ni)	
	r / nm	*N*
0.5mol/l Na_2MoO_4+0.5mol/l $NiSO_4$ + 1.0mol/l Na_3 cit. sol.	0.331	1.4

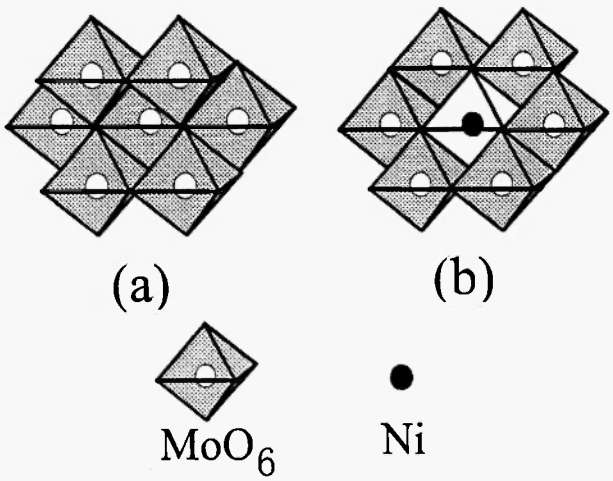

Fig. 12: Schematic drawings of the structural models of poly-molybdate in (a) 1.0 mol/l Na_2MoO_4, and (b) 0.5 mol/l Na_2MoO_4 + 0.5 mol/l $NiSO_4$ aqueous solutions.

containing Mo, Ni and citric ions /40/. In such solutions, molybdenum ions exist as small molybdate ions which probably form citric complexes. Consequently, it may safely be concluded that these small Mo(VI)-citrate complexes play a significant role in the mechanism of the induced codeposition.

6. CONCLUDING REMARKS

The fundamentals of the AXS method were explained with not only a simple example of the hydration structure in concentrated $ZnCl_2$ solutions, but also a couple of complicate solution systems of the ferric hydroxide gel in solution and poly-molybdate ions in acid Mo-Ni solutions. The potential capability of the AXS method to investigate the structure around a heavy metallic ion in aqueous solution has clearly been demonstrated and the present authors maintain the view that the AXS method is very promising for structural characterization of various types of aqueous solutions.

ACKNOWLEDGEMENTS

Some results described in this review were supported by Grant-in-Aid for Scientific Research, the Ministry of Education, Science and Culture (No.09212216 & No.09305052). We particularly thank the staff in the photon factory, High Energy Accelerator Research Organization, Professor M. Nomura and Dr A. Koyama. The authors are grateful to Professors Y. Awakura, Y. Waseda and T. Hirato for their interest in

these works and for helpful discussions. One of the authors (KS) also thanks the Japan Society for the Promotion of Science for Research Fellowships.

REFERENCES

1. S. Hosoya, *Bull. Phys. Soc. Japan*, **25**, 110 (1970).
2. N. J. Shevchik, *Phil. Mag.*, **35**, 805 (1977).
3. P. H. Fuoss, P. Eisenberger, W. K. Warburton and A. Bienenstock, *Phys. Rev. Lett.*, 46, 1537 (1981).
4. E. Matsubara, K. Harada, Y. Waseda and M. Iwase, *Z. Naturforsch.*, **43a**, 181 (1988).
5. Y. Waseda, *Novel Application of Anomalous X-ray Scattering for Structural Characterization of Disordered Materials*, Springer-Verlag, Heidelberg, p.87, (1984).
6 E. Matsubara and Y. Waseda, *J. Phys.: Condens. Matter*, 1, 8575 (1989).
7. E. Matsubara, K. Okuda and Y. Waseda, *J. Phys.: Condens. Matter*, 2, 9133 (1990).
8. K. Shinoda, E. Matsubara, A. Muramatsu and Y. Waseda, *Mat. Trans. Jpn. Inst. Metals*, **35**, 394 (1994).
9. K. Shinoda, E. Matsubara, M. Saito, Y. Waseda, T. Hirato and Y. Awakura, *Z. Naturforsch.*, 52a, 855 (1997).
10. D.T. Cromer and D. Lieberman, *J. Chem. Phys.*, **53**, 1891 (1970).
11. K. Shinoda, K. Sugiyama and Y. Waseda, *High Temp. Mat. Proc.*, 14, 75 (1995).
12. E. Matsubara, Y. Waseda, M. Mitera and T. Masumoto, *Trans. Jpn. Inst. Metals*, 29, 697 (1988).
13. E. Matsubara and Y. Waseda, *Resonant Anomalous X-ray Scattering, Theory and Applications*, eds. G. Materlik, C.J. Sparks and K. Fischer, North-Holland, Amsterdam (1994), p. 345.
14. A.H. Narten and H.A. Levy, *Science*, **165**, 447 (1969).
15. J.E. Enderby and G.W. Neilson, *Adv. Phys.*, 29, 323 (1980).
16. P. Lagarde, A. Fontaine, D. Raoux, A. Sadoc and P. Migliardo, *J. Chem. Phys.*, 72, 3061 (1980).
17. K.F. Ludwig, Jr., W.K. Warburton and A. fontaine, *J. Chem. Phys.*, 87, 620 (1987).
18. D.L. Wertz, R.M. Lawrence and R.F. Kruh, *J. Chem. Phys.*, 43, 2163 (1965).
19. D.L. Wertz and R.F. Kruh, *J. Chem. Phys.*, **50**, 4313 (1969).
20. H. Ohtaki, T. Yamaguchi and M. Maeda, *Bull. Chem. Soc. Jpn.*, 49, 701 (1976).
21. R. Caminiti and P. Cucca, *Chem. Phys. Lett.*, 89, 110 (1982).
22. R.A. Howe, W.S. Hawells and J.E. Enderby, *J. Phys. C: Solid State Phys.*, 7, L111 (1974).
23. M.A. Blesa and E. Matijevic, *Adv. Colloid Interface Sci.*, 29, 173 (1989).
24. A.H. Narten and H.A. Levy, *Science*, 160, 447 (1969).
25. A.H. Narten, *J. Chem. Phys.*, 56, 1905 (1972).
26. E. Matsubara, K. Sugiyama, Y. Waseda, M. Ashizuka and E. Ishida, *J. Mat. Sci. Lett.*, 9, 14 (1990).
27. V.Q. Kinh, E. Chassaing and M. Saurat, *Electrodep. Surf. Treat.*, 3, 205 (1975).
28. I.A. Raj, *J. Mat. Sci.*, 28, 4375 (1993).
29. A. Brenner, *Electrodeposition of Alloys*, 2, Chap. 34, Academic Press, Inc., New York (1963).
30. D.W. Ernst and M.L. Holt, *J. Electrochem. Soc.*, 105, 686 (1958).
31. S. Rengakuji, Y. Nakamura, M. Inoue, K. Nishibe and H. Imanaga, *Denki Kagaku*, 59, 885 (1991).
32. H. Fukushima, T. Akiyama, S. Akagi and K. Higashi, *Trans. Jpn. Inst. Metals*, 20, 358 (1979).
33. E.J. Podlaha, M. Matlosz and D. Landolt, *J. Electrochem. Soc.*, 140, L149 (1993).
34. E.J. Podlaha and D. Landolt, *J. Electrochem. Soc.*, 143, 885 (1996).
35. L. Kihlborg, *Arkiv för Kemi*, 21, 357 (1963).
36. K. Sjobom and B. Hedman, *Acta Chem. Scand*, 27, 3673 (1973).
37. F.A. Cotton and G. Wilkinson, *Advanced Inorganic Chemistry*, 5th ed., Interscience-Wiley, New York (1988), p. 817.
38. G. Johansson, L. Pettersson and N. Ingri, *Acta Chem. Scand.*, A28, 1119 (1974).
39. A. Perloff, *Inorg. Chem.*, 9, 2228 (1970).
40. T. Watanabe, T. Naoe, A. Mitsuo and S. Katsumata, *J. Finish. Soc. Jpn.*, 40, 458 (1989).